Solution Combustion Synthesis of Rare Earth Orthoferrite Nanoparticles: a Comparative Study on Multiferroic Properties of Er–FeO_3 vs (La,Yb)FeO_3

P. Sathish Kumar, I. Phebe Kokila, M. Kanagaraj, Anil Kumar Paidi, Liang He, Helen Annal Therese & S. Madeswaran

Journal of Superconductivity and Novel Magnetism

ISSN 1557-1939

J Supercond Nov Magn
DOI 10.1007/s10948-020-05625-9

Springer

Journal of Superconductivity and Novel Magnetism
https://doi.org/10.1007/s10948-020-05625-9

ORIGINAL PAPER

Solution Combustion Synthesis of Rare Earth Orthoferrite Nanoparticles: a Comparative Study on Multiferroic Properties of Er–FeO_3 vs (La,Yb)FeO_3

P. Sathish Kumar[1] · I. Phebe Kokila[2] · M. Kanagaraj[3] · Anil Kumar Paidi[4] · Liang He[3,5] · Helen Annal Therese[2,6] · S. Madeswaran[1]

Received: 15 June 2020 / Accepted: 21 July 2020

Abstract

Rare earth (RE = La, Er, and $YbFeO_3$) ferrites are prepared from their nitrate precursors using the solution combustion method. Structural analysis using powder X-ray diffraction (XRD) technique indicates that the synthesized La-, Er-, and Yb–FeO_3 perovskite nanoparticles have pure phase orthorhombic super unit cells. The XRD patterns of Er–FeO_3 and Yb–FeO_3 are found to be indexed in Pbnm (62) space group with cell dimensions in the range of a_o = 5.2611–5.2784 Å, b_o = 5.5729–5.5898 Å, and c_o = 7.596–7.6002 Å, while the space group of Pnma (62) with a_o = 5.5688 Å, b_o = 7.8523 Å, and c_o = 5.5542 Å are obtained for $LaFeO_3$. Surface morphological studies show aggregated spherical-shaped nanoparticles having an orthorhombic crystal structure with an average particle size of ~ 50 nm. Magnetic properties of all the three RE ferrite synthesized in this work exhibit antiferromagnetic behavior. The study of dielectric properties of all the three RE ferrites shows dispersive behavior at low frequencies with low loss. Temperature-dependent dielectric studies confirm that the antiferromagnetic-paramagnetic transition temperature appears at 445 K. A larger P-E loop with a squareness ratio of 1.583 for $ErFeO_3$ orthoferrites suggests that it is more advantageous than $LaFeO_3$ and $YbFeO_3$ for making modern electronic devices.

Keywords Orthoferrites · Solution combustion · Multiferroism · Electric coupling · Piezoelectric polarization

1 Introduction

Rare earth ferrites (RE-FeO_3) also known as multiferroic materials crystallize in the orthorhombic structure gained remarkable attention in recent years due to their unusual but interesting coexistence of ferroelectric and weak ferromagnetic coupling. Although the magnetoelectric coupling phenomenon does not naturally exist in RE ferrites, often, not only was it realized through the structural or electronic modification, but it also shows various exceptional effects such as spin reorientation, compensation effect, antisymmetric exchange interaction, Dzyaloshinsky-Moriya type canting effect, non-centrosymmetric distortion of Fe-spins, and magnetocrystalline anisotropy [1, 2]. RE ferrites were found suitable in a wide range of applications such as magnetic data storage, magneto-optic devices, magnetocaloric refrigerators, magnetoresistive detectors, electrocaloric sensors, gas separators, electrocatalysis, and spintronic devices [3, 4]. In general, the synthesis method adapted for RE-FeO_3 by many research groups involves high-temperature solid-state reaction which requires the reaction temperature to be maintained above 1300 °C [5]. Despite various preparative methods including reactive milling,

✉ S. Madeswaran
madeswaran.s@vit.ac.in

[1] Department of Physics, School of Advanced Sciences, Vellore Institute of Technology, Vellore 632014, India

[2] Nanotechnology Research Centre, SRM Institute of Science and Technology, Kattankulathur, Kancheepuram, Tamil Nadu 603203, India

[3] School of Electronic Science and Engineering, Nanjing University, Nanjing 210093, People's Republic of China

[4] Department of Metallurgical Engineering and Materials Science, Indian Institute of Technology Bombay, Powai, Mumbai 400076, India

[5] York-Nanjing Joint Centre for Spintronics and Nano Engineering (YNJC), School of Electronics Science and Engineering, Nanjing University, Nanjing 210093, People's Republic of China

[6] Department of Chemistry, SRM Institute of Science and Technology, Kattankulathur, Kancheepuram, Tamil Nadu 603203, India

Published online: 03 August 2020

sonochemical, and co-precipitation employed for synthesizing RE- ferrites, they are all seemingly not much feasible due to two reasons: the appearance of secondary impurity phase difficulty in maintaining the precise concentration of doping ratios [6–9]. On the other hand, the solution combustion synthesis (SCS) method requires low reaction temperature compared to conventional solid-state synthesis methods, which has attracted researchers' attention in recent years. Li et al. [5] reported the advantages of the SCS method over other methods wherein the precursor metal salts (nitrates, carbonates, sulfates) act as oxidants, and the fuels (citric acid, amylum, glycine, urea, sucrose) act as reducing agents during the exothermal redox reaction [10]. Due to less time consumption, low reactive temperatures, precise control of doping concentrations, and flexibility in selecting oxidants/reducing agents, SCS is preferable for synthesizing the RE-FeO_3 system [11]. In this work, we report the synthesis of RE-FeO_3 (RE = La, Er, and Yb) orthoferrites using the SCS method and study their interactive behavior correlated to the structural, dielectric, magnetic, and ferroelectric properties. It is worthy to note that a search of the literature shows that the present work seems to be the first report on the property study of $ErFeO_3$ synthesized by the SCS method.

A comparison of the structural, magnetic, and dielectric properties of $ErFeO_3$ against $LaFeO_3$ and $YbFeO_3$ is presented. $ErFeO_3$ showed superior structural, magnetic, and dielectric properties compared with $LaFeO_3$ and $YbFeO_3$ [8, 12–15].

2 Experimental Details

2.1 Material Synthesis

RE-FeO_3 (RE = La, Er, Yb) nanoparticles were synthesized by the solution combustion (SC) method using citric acid as an effective fuel agent. High-purity (> 99%) La $(NO_3)_3{\cdot}6H_2O$, $Er(NO_3)_3{\cdot}5H_2O$, $Yb(NO_3)_3{\cdot}6H_2O$, and Fe $(NO_3)_3{\cdot}9H_2O$ chemicals were used as the starting materials. Starting precursors of $A(NO_3)_3{\cdot}xH_2O$ (A = La, Er, Yb) and $Fe(NO_3)_3{\cdot}9H_2O$ were dissolved in the desired quantity of distilled water, and citric acid drops were then added with continuous stirring (see Table 1). After the dissolution of all the salts, the temperature of the solution was raised to 60 °C in 10–15 min and continued stirring until a "clear solution" was formed. The resultant clear solution was placed in the muffle furnace with the help of alumina crucible and heated to its decomposing point of 400 °C. $LaFeO_3$, $ErFeO_3$, and $YbFeO_3$ powders (in brown color) were obtained by sintering

Table 1 Quantity of starting materials used in the synthesis of $LaFeO_3$, $ErFeO_3$, and $YbFeO_3$

S. No.	Molecular formula	Molecular weight	Weighed quantity for preparation
1	$Fe(NO_3)_3{\cdot}9H_2O$ (1 M)	404.00	4.04 g/10 ml
2	Yb $(NO_3)_3{\cdot}5H_2O$ (1 M)	449.13	4.5 g/10 ml
3	Er $(NO_3)_3{\cdot}5H_2O$ (1 M)	443.35	4.44 g/10 ml
4	La $(NO_3)_3{\cdot}6H_2O$ (1 M)	433.01	4.33 g/10 ml
5	$C_6H_8O_7$(1.67 M)	192.13	3.2 g/10 ml

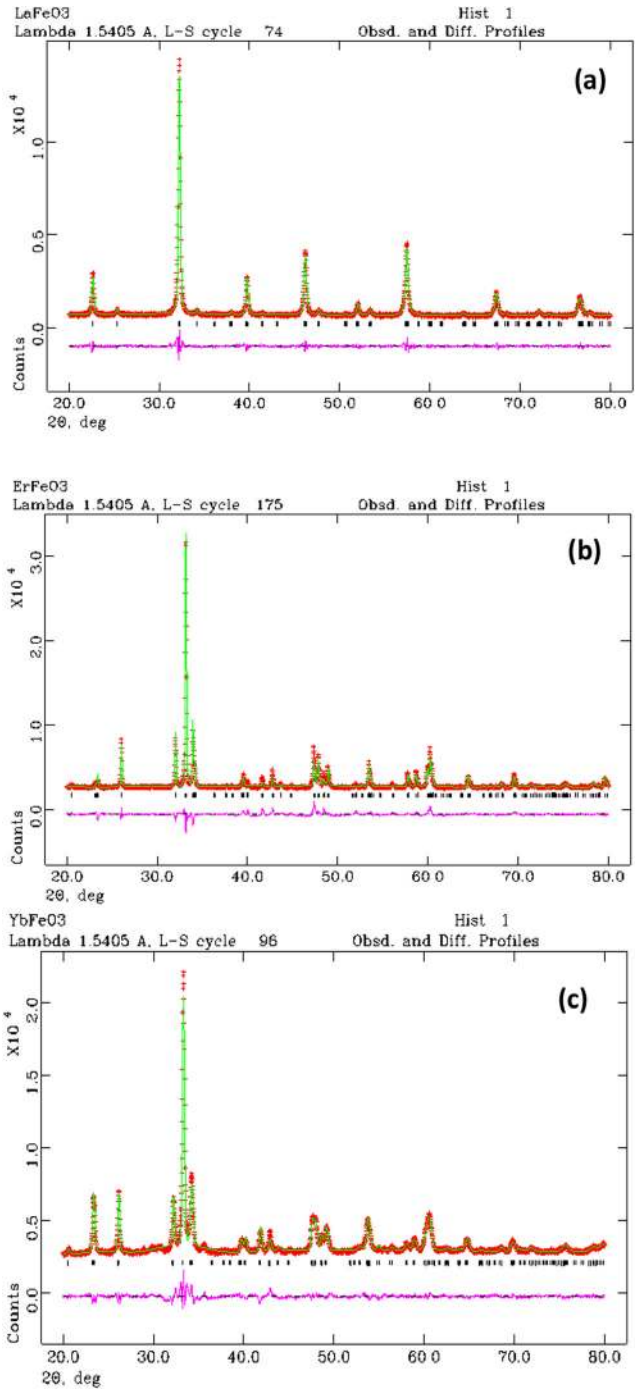

Fig. 1 **a**–**c** Final Rietveld XRD data plot of **a** $LaFeO_3$, **b** $ErFeO_3$ and **c** $YbFeO_3$ compounds (red, observed; green, calculated; black, vertical bars—positions of the Bragg reflections; pink, the difference between observed and calculated intensities)

Table 2 Crystallographic data table of the $LaFeO_3$, $ErFeO_3$, and $YbFeO_3$ compounds derived from Rietveld refinement of high-resolution X-ray diffractogram ($\lambda = 1.540\ 56$ Å) data collected at 300 K

Compound	$LaFeO_3$	$ErFeO_3$	$YbFeO_3$
Formula weight	242.75	271.11	276.89
Crystal system	Orthorhombic	Orthorhombic	Orthorhombic
Space group (No.)	*Pnma* (*62*)	*Pbnm* (*62*)	*Pbnm* (*62*)
a (Å)	5.5688(1)	5.2784(3)	5.2611(2)
b (Å)	7.8523(3)	5.5898(3)	5.5729(2)
c (Å)	5.5542(3)	7.6002(1)	7.596(3)
β (°)	–	–	–
V (Å^3)	242.875(1)	224.252(6)	222.72(10)
Z	4	4	4
Temperature (K)	293(2)	293(2)	293(2)
wRp/ Rp	0.0581/0.0458	0.0442/0.0316	0.0376/0.0270
Chi^2 value	3.007	5.958	4.709

respectively at 500 °C, 750 °C, and 900 °C for 2 h inside a tubular furnace in open air.

2.2 Material Characterization

The powder X-ray diffraction (XRD) patterns of $LaFeO_3$, $ErFeO_3$, and $YbFeO_3$ compounds were recorded on a Bruker D8 Advanced powder X-ray diffractometer using Cu Kα ($\lambda = 1.5406$ Å) radiation. The slow-scan powder XRD data for the title compounds were gathered with a step size of 0.02° and a step time 3 s, in the 2θ range of 20–90°. DIAMOND 3.0 graphic software was employed for the crystal structure visualization. Rietveld refinement was performed on diffraction intensity data of $LaFeO_3$, $ErFeO_3$, and $YbFeO_3$ compounds using the GSAS program with the EXPGUI front-end. Surface morphology and elemental composition of the compounds were studied with field emission scanning electron microscopy (FESEM, Philips FEI Quanta-200f)) equipped with elemental dispersive spectroscopy (EDS, Bruker instruments). Magnetic field-dependent magnetization measurements were performed in vibrating sample magnetometer (VSM, Lakeshore, 7407, USA). A HIOKI 3532-50 LCR controller (Japan) was used to study the dielectric properties and ferroelectric hysteresis (P-E loop) of pelletized nano-crystalline powders.

3 Results and Discussion

3.1 Crystal Structure

The Rietveld refined plots of the as-synthesized compounds $LaFeO_3$, $ErFeO_3$, and $YbFeO_3$ compounds were obtained using a GSAS powder X-ray diffraction tool (Bruker D8 advance). Rietveld refinement was performed by fitting the peak profiles using the Pseudo-Voigt function, while all the systems contain the room temperature orthorhombic structure with a space group of Pnma/Pbnm (62). The starting refinement models were taken from the ICSD database No. 37-1493, No. 72-1281, and No. 46-0136 for $LaFeO_3$, $ErFeO_3$, and $YbFeO_3$, respectively. The experimentally observed structural pattern and theoretically computed Rietveld refined patterns are depicted in Fig. 1a–c, and detailed crystallographic data are summarized in Table 2. The calculated cell parameters were in correlation with that of the theoretical one deduced from Rietveld analysis. The diffractograms indicate that the $LaFeO_3$, $ErFeO_3$, and $YbFeO_3$ compounds have an orthorhombic crystal structure with primitive lattice that belongs to the space group Pnma/Pbnm (62). A

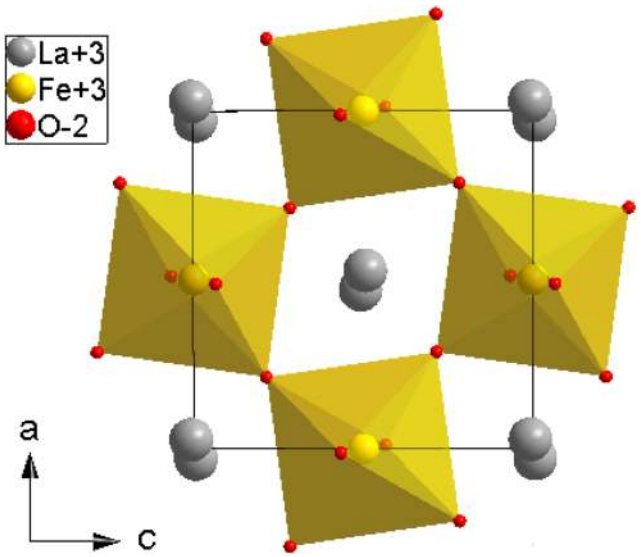

Fig. 2 Polyhedral representation of the unit cell of $LaFeO_3$ orthorhombic crystal structure (space group: *Pnma* (62)) is illustrated having FeO_6 octahedra (yellow) and La atoms (gray)

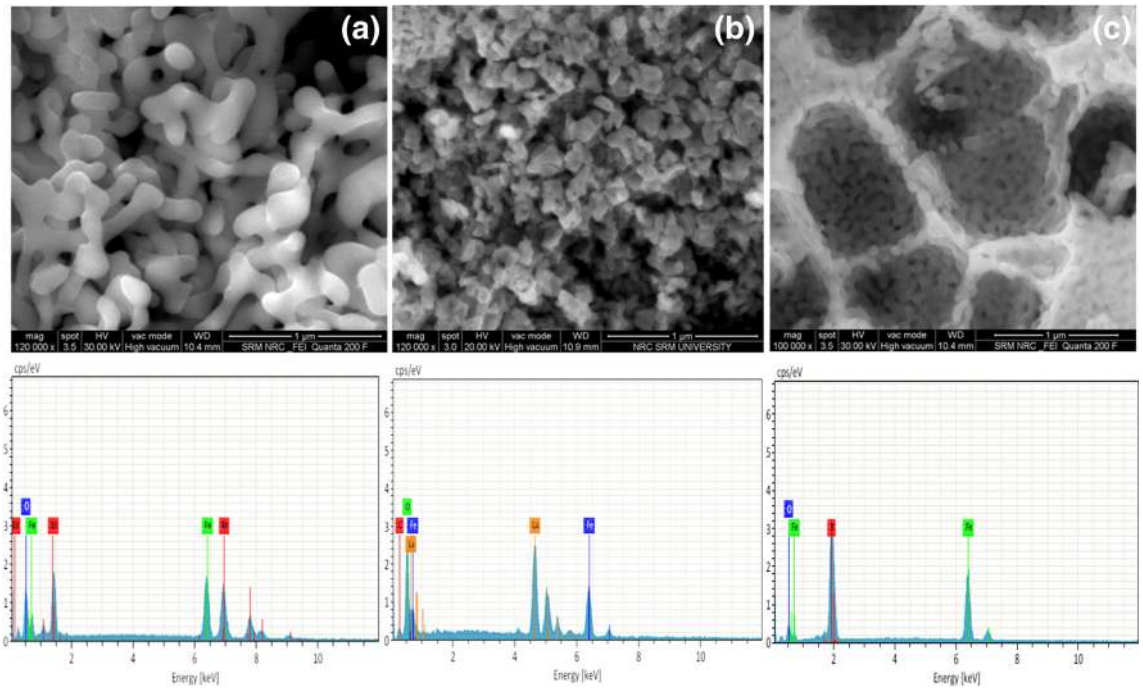

Fig. 3 **a**–**c** FESEM images and corresponding EDX results acquired for **a** $LaFeO_3$, **b** $ErFeO_3$, and **c** $YbFeO_3$

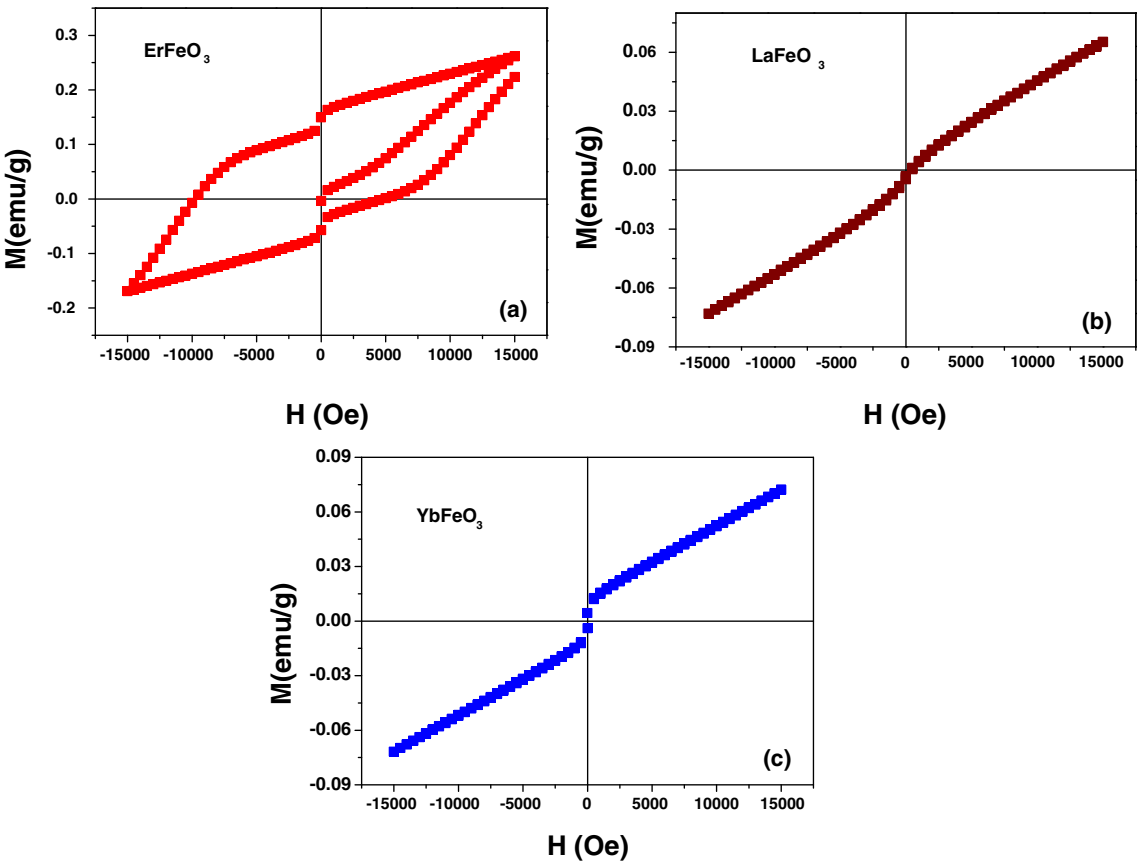

Fig. 4 **a**–**c** Magnetization hysteresis (M-H) loops obtained at room temperature for **a** $ErFeO_3$, **b** $LaFeO_3$, and **c** $YbFeO_3$

representative $LaFeO_3$ unit cell derived from Diamond software is displayed in Fig. 2 depicting the La atom (gray) along the (010) direction surrounded by the Fe octahedra (yellow) of the unit cell. The splitting of reflection at 33° becomes more prominent with the decrease of RE-site ionic radii, which denotes the orthorhombic structure with a reduction of RE^{3+}-site ions [10]. The average crystallite sizes (D) calculated using the Debye-Scherrer relation were found to be ~ 36, ~ 56, and ~ 37 nm for the $LaFeO_3$, $ErFeO_3$, and $YbFeO_3$, respectively. The lattice strain component for $ErFeO_3$ was a little lower (0.0023) when compared with $LaFeO_3$ and $YbFeO_3$ [10].

3.2 FESEM (Microstructure) and EDX (Elemental) Analysis

Figure 3 a–c depict field emission scanning electron microscopic (FESEM - Philips FEI Quanta-200f) images of $LaFeO_3$, $ErFeO_3$, and $YbFeO_3$ compounds scanned in 1-μm-scale resolution. Whilst all the three compounds show agglomerated and aggregated particles scaling around > 500 nm, $LaFeO_3$ has a relatively smaller particle size in comparison with $ErFeO_3$ and $YbFeO_3$. $YbFeO_3$, in fact, exhibits a unique matrix of particles homogeneously distributed with large trenches-like structure. The energy-dispersive spectrum (EDX) in Fig. 3d–f shows the constituting elements and their quantification as per the stoichiometry expected to be 1:1:3 ratio. In $LaFeO_3$, the estimated atomic percentages of La, Fe, and O were 11.66%, 15.53%, and 66.50% with addition of a small amount of carbon presented as 6.31%. Similarly, they are 13.36%, 14.41%, and 72.23% for $ErFeO_3$, while for $YbFeO_3$, those values are 18.57%, 12.05%, and 69.38% which have been theoretically in agreement with the EDX experimental values.

3.3 VSM Magnetic Response Analysis

Field-dependent magnetization at room temperature (300 K) measurement was carried out for the $ErFeO_3$, $LaFeO_3$, and $YbFeO_3$ samples (VSM, Lakeshore, 7407, USA), and the magnetic response deciphered is shown in Fig. 4a–c. Er exhibits antiferromagnetic (AFM) behavior at 300 K and a negligible magnetic saturation (M_s), which agrees with the previous report by Ramu et al. [11], indicating the unusual non-symmetric

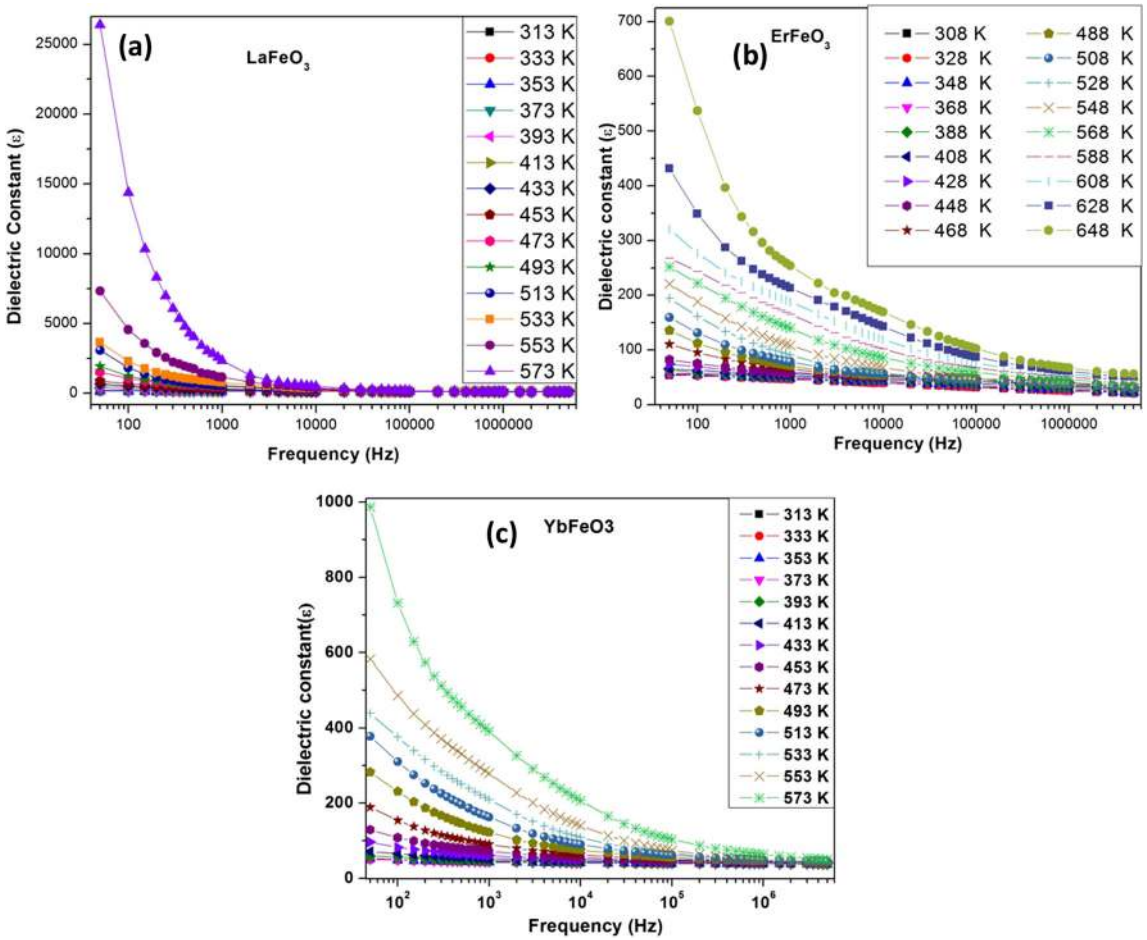

Fig. 5 **a**–**c** Dielectric constant vs frequency graph for **a** $LaFeO_3$, **b** $ErFeO_3$, and **c** $YbFeO_3$

negative magnetization at lower temperatures (5 K). On the other hand, La and Yb show a similar antiferromagnetic nature where the interpenetrating magnetic sublattices of RE and Fe ions align in the antiparallel direction. The magneton number (μ_B) was calculated from the magnetic field-dependent isotherms (300 K) from the relation $\mu_B = [M_w \times M_s] / 5585$, where M_w refers molecular weight of the ferrite composition, M_s refers to saturation magnetization (emu/g), and 5585 is the magnetic factor. Here, the huge μ_B values with high coercivity for the Er than La and Yb may be attributed to the dominance of super-exchange interaction between atoms occupying the tetrahedral (RE = La, Er, Yb) and octahedral Fe (B) sites over the magnetic nature contributed by the unpaired 3d electrons and the uneven distribution of atoms in the A and B sites of the orthorhombic lattice [10, 11, 13, 16–19].

The hysteresis loop of $ErFeO_3$ exhibited a triangular shape at the lower applied field, which is due to the presence of domain walls in the sample. This kind of behavior was termed as "domain theory," where the triangular shape in the M-H loop occurs in orthoferrites due to the presence of a few domain walls even after saturation [20]. The triangular shape is correlated to the energy required to remove the existing domain walls on increasing the magnetic field. The triangular shape or step-like behavior occurring after remanence is the amount of field required for the formation of domain walls again through a single domain rotation. A similar kind of observation was reported by Tsymbal et al. at a temperature below the compensation temperature [20]. The influence of domain wall theory on the shape of the M-H loop is further extended to a temperature above the compensation temperature. It can be concluded that Er nanoparticles exhibited weak ferromagnetic behavior at room temperature with the step-like increase due to the transformation from multi-domain to single domain by irreversible rotation. However, other the La and Yb orthoferrites did not have domain wall rotation, perhaps a non-collinear antiferromagnetic (AFM) nature. Spin interaction in the magnetic sublattice led to the weakly dependent magnetic saturation and coercivity than Er under given magnetic field.

3.4 Dielectric Study

The variation of dielectric constant with frequency obtained for $LaFeO_3$, $ErFeO_3$ and $YbFeO_3$ samples is shown in Fig. 5a–c. All the samples exhibited high

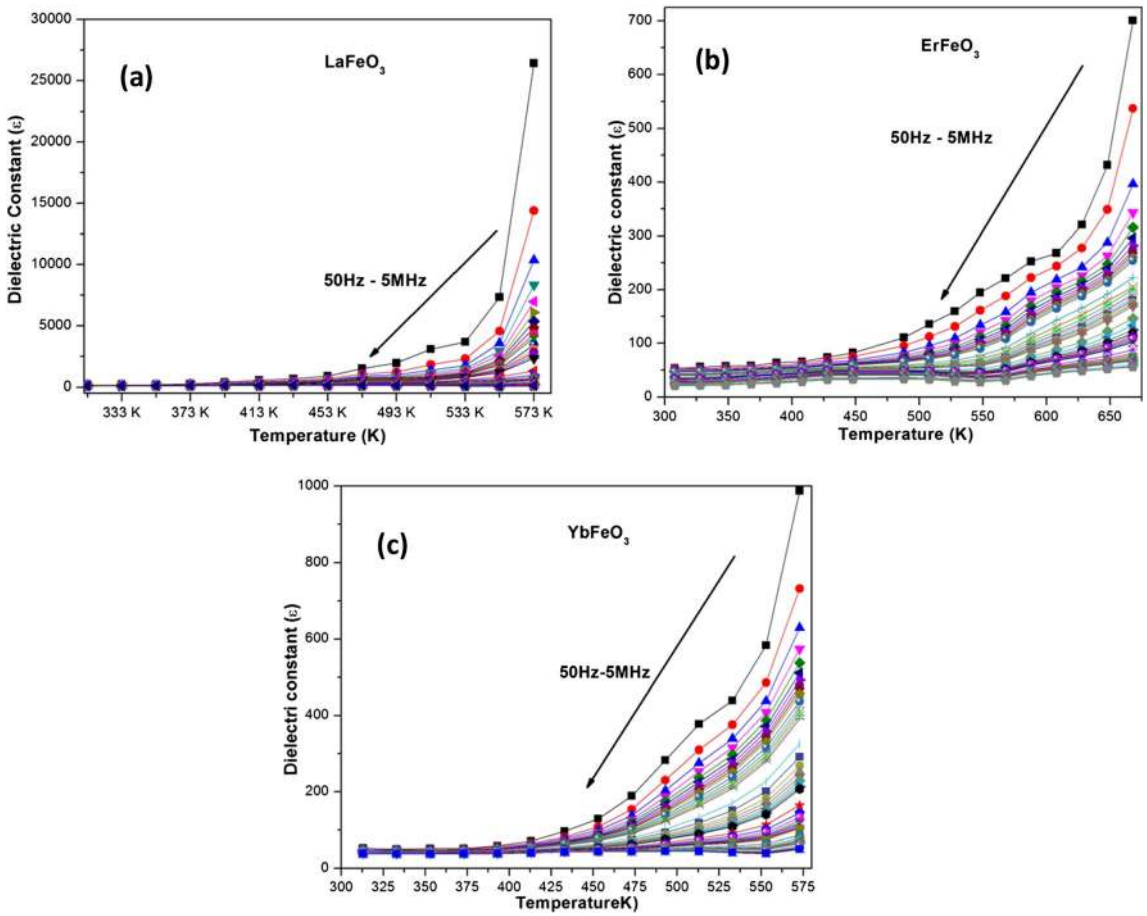

Fig. 6 **a**–**c** Temperature-dependent dielectric constant of **a** $LaFeO_3$, **b** $ErFeO_3$, and **c** $YbFeO_3$

dielectric constant at a lower frequency range that confirmed the presence of electrode polarization effect. The variation of dielectric constant with temperature Fig. 6a–c clearly indicates the presence of dielectric relaxation in the samples at the high-temperature regime. This phenomenon was apparent in ferrites which confirmed the Maxwell-Wagner–type interfacial polarization due to the local displacement of electrons through the exchange of $Fe^{2+} \leftrightarrow Fe^{3+}$ ions [4]. The increase of dielectric constant $\varepsilon' = 25{,}000$ at a lower frequency for La compared to Er and Yb suggests the increase of exchange of Fe ions which is in line with the previous reports [14, 15, 19, 21]. Nevertheless, the convergence and saturated flat line observed at the lower frequencies could be due to the electronic polarization where the electric dipoles tend to get disoriented with rapid change in the applied ac electric field [2, 11, 14, 22].

Dielectric response occurring around ~200 K in ferrites implies the thermally activated polaron relaxation stimulated by the hopping motions of charge carriers between d band metal ions Fe^{2+} and Fe^{3+}. Among the various types of anomalies (interfacial (Pi), dipolar (Pd), atomic (Psc), and electronic (Pe)), the interfacial and dipolar polarization is primarily responsible for the rapid increase in dielectric constant concerning higher temperatures. The dielectric loss with temperature variation for various frequency ranges is demonstrated in Fig. 7a–c. The figure represents the presence of dielectric relaxation which is associated with the oxygen vacancies induced by high-temperature sintering. This behavior is also associated with the Maxwell-Wagner relaxation phenomena present in the samples.

3.5 PE Loop-Ferroelectric Analysis

Figure 8 a–c show the polarization-electric field loop (P-E loop) measured in terms of the electric field (V/m) while varying the electric polarization (C/m^2) for the $ErFeO_3$, $LaFeO_3$ and $YbFeO_3$ samples, and electric polarization parameters such as coercive field (Ec), remanence (Pr), and maximum polarization (Pm) are listed in Table 3. The squareness ratio of the PE hysteresis of

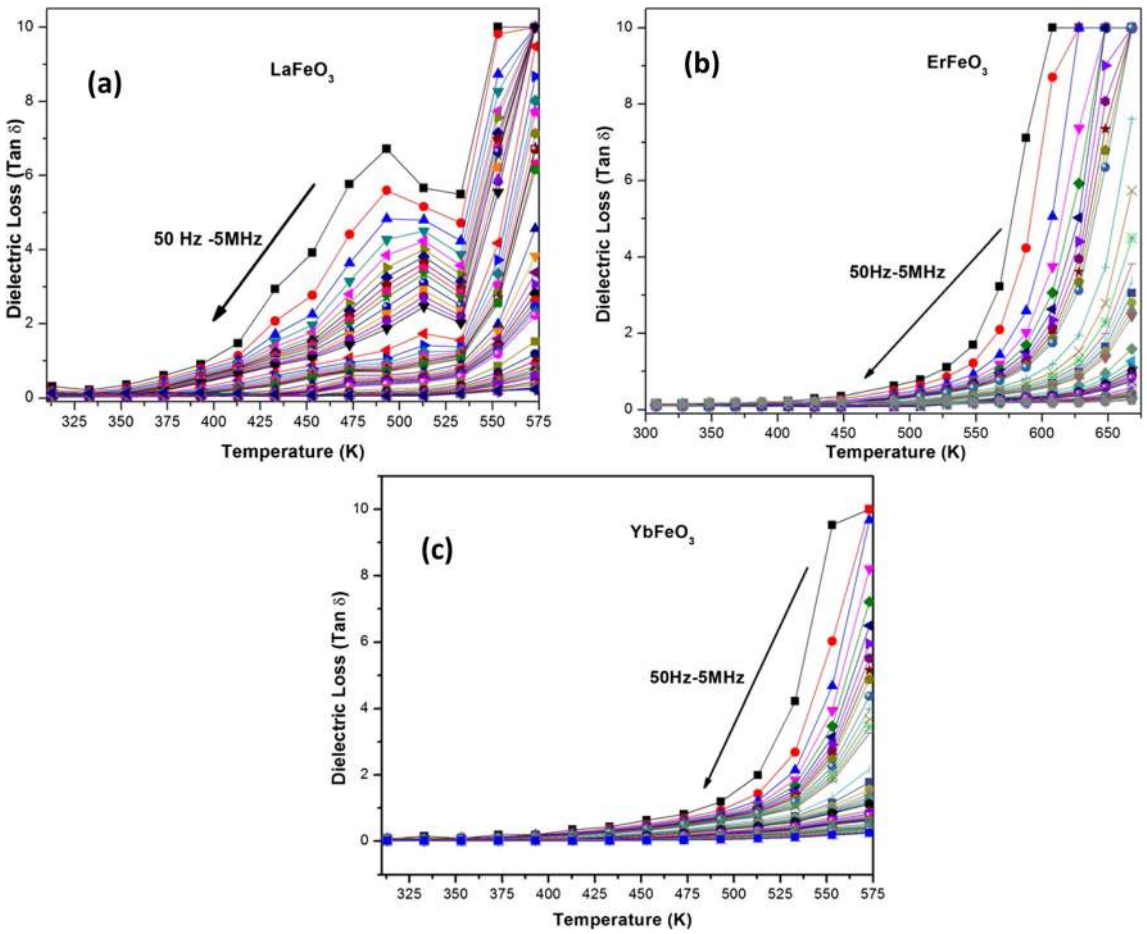

Fig. 7 **a**–**c** Dielectric loss as a function of temperature for **a** $LaFeO_3$, **b** $ErFeO_3$, and **c** $YbFeO_3$

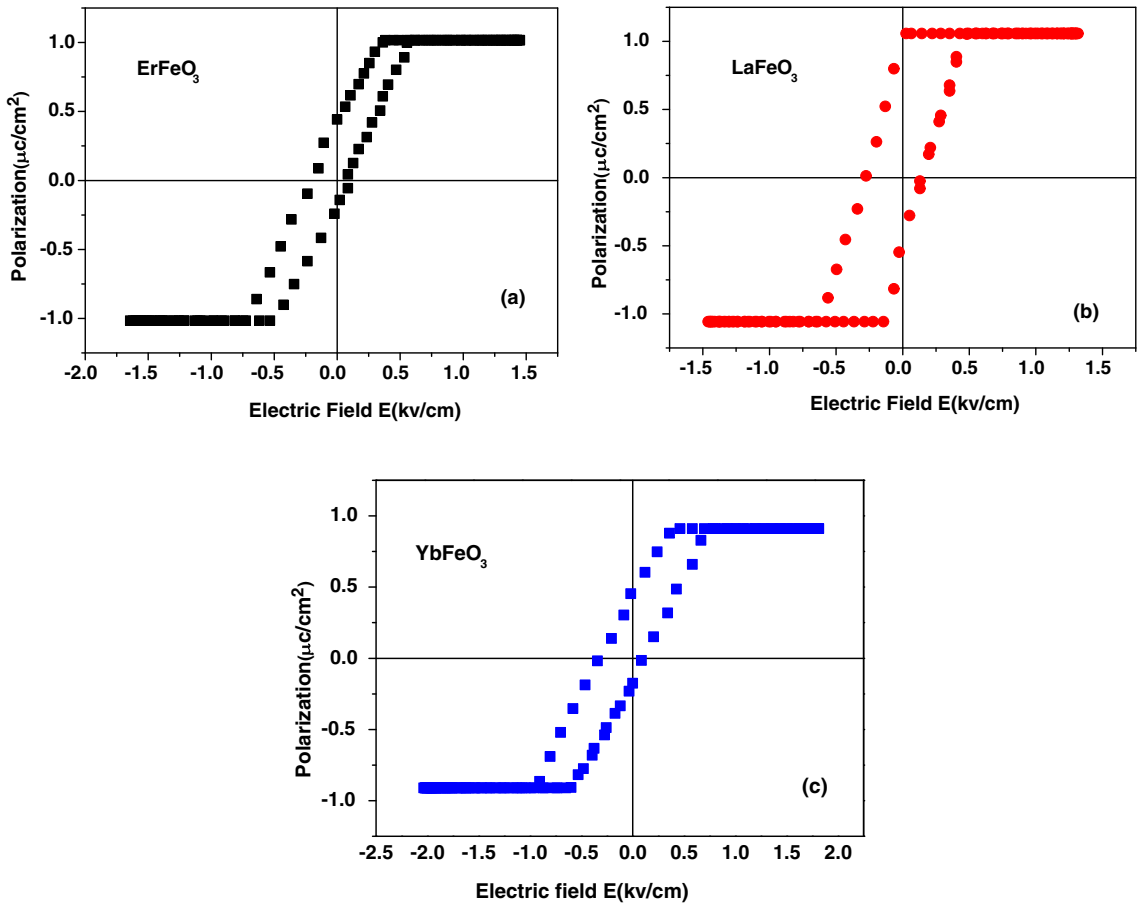

Fig. 8 **a**–**c** Ferroelectric hysteresis loops of **a** $ErFeO_3$, **b** $LaFeO_3$, and **c** $YbFeO_3$ measured at 300 K

$ErFeO_3$ was calculated to be 1.583 which was remarkably larger than for the $LaFeO_3$ and $YbFeO_3$ samples. The strong frequency dependence of dielectric constant shows the relaxor-ferroelectric behavior in the samples which is ascertained by the weak Pr values obtained, especially at a very low-frequency range. The anisotropy is inherently weaker as the ceramics tend to behave as a relaxor-ferroelectric and exhibits the piezoelectric nature while being subjected to local strain effect during electrical polarization [22]. By the above comparison, solution combustion–assisted $ErFeO_3$ was found to have a major advantage over the other two orthoferrites due to its better sequential multiferroic characteristics associated with its particle size than $LaFeO_3$ and $YbFeO_3$.

Table 3 The ferroelectric experimental data of $LaFeO_3$, $ErFeO_3$, and $YbFeO_3$ compounds

Sample	Coercive field (E_c) (kV/mm)	Remanence (P_r) ($\mu C/cm^2$)	Max. polarization (P_m) ($\mu C/cm^2$)	Squareness (P_r/P_m)
$LaFeO_3$	0.208	0.532	1.057	0.503
$ErFeO_3$	0.723	1.609	1.016	1.583
$YbFeO_3$	0.861	0.324	0.910	0.356

4 Conclusion

Phase-pure $LaFeO_3$, $ErFeO_3$, and $YbFeO_3$ orthoferrites were synthesized by the solution combustion method. XRD study confirmed pure orthorhombic structure with a space group of Pnma/Pbnm (62) in all the three orthoferrite samples, and a more prominent splitting of reflection at 33° with the decrease in R-site ionic radii was observed. Unusual non-symmetric paramagnetic nature was realized in $ErFeO_3$, whereas $LaFeO_3$ and $YbFeO_3$ revealed the antiferromagnetic type of magnetism. Frequency-dependent dielectric constant showed dispersive behavior at low frequencies with low losses. Temperature-dependent dielectric constant displayed an anomaly around 445 K, perhaps due to the antiferromagnetic to paramagnetic transition caused by the change in polarization. The $ErFeO_3$ exhibited a larger P-E loop squareness ratio of 1.583 than $LaFeO_3$ and $YbFeO_3$. The weak Pr values at a very low-frequency range showed the relaxor-ferroelectric behavior and the

piezoelectric nature due to strain/stress induction during an electrical polarization.

Acknowledgments The authors would like to thank Vellore Institute of Technology, Vellore management, for their continuous support and encouragement to carry out the research and development works, and Mrs. M.V. Beena, IITM, Chennai, for providing the VSM facilities to perform the magnetic characterization study.

References

1. Grant, R.W., Geller, S.: Mechanism of spin reorientation in $ErFeO_3$. Solid State Commun. **7**(18), 1291–1294 (1969)
2. Kreisel, J., Kenzelmann, M.: Multiferroics-the challenge of coupling magnetism and ferroelectricity. Europhys. News. **40**(5), 17–20 (2009)
3. Chen, Z.-X., Chen, Y., Jiang, Y.-S.: Comparative study of ABO_3 perovskite compounds. 1. $ATiO_3$ (A= Ca, Sr, Ba, and Pb) perovskites. J. Phys. Chem. B. **106**(39), 9986–9992 (2002)
4. Serrao, C.R., Sahu, J.R., Ramesha, K., Rao, C.N.R.: Magnetoelectric Effect in Rare Earth Ferrites, LnFe 2 O 4. AIP (2008)
5. Li, F.-T., Ran, J., Jaroniec, M., Qiao, S.Z.: Solution combustion synthesis of metal oxide nanomaterials for energy storage and conversion. Nanoscale. **7**(42), 17590–17610 (2015)
6. Hwang, Y., Kang, D.S., Park, M.H.: Solution combustion synthesis and surface properties of $LaFeO_3$ powders. J. Ceram. Process. Res. **11**(3), 397–400 (2010)
7. Shen, H., Cheng, G., Wu, A., Xu, J., Zhao, J.: Combustion synthesis and characterization of nano-crystalline $LaFeO_3$ powder. Phys. Status Solidi A. **206**(7), 1420–1424 (2009)
8. Venkaiah, G., Rao, K.V., Kumar, V.S.S., Chakra, C.H.S.: Solution combustion synthesis and characterization of nano-crystalline lanthanum ferrite using glycine as a fuel. Int. J. Mater. Methods Technol. **1**(1), 01–07 (2013)
9. Zaza, F., Pallozzi, V., Serra, E., Pasquali, M.: Combustion synthesis of $LaFeO_3$ sensing nanomaterial. In, 2015, p. 020003. AIP Publishing
10. Raghuvanshi, S., Satalkar, M., Tapkir, P., Ghodke, N., Kane, S.N.: On the structural and magnetic study of $Mg_{1-x}Zn_xFe_2O_4$. In, 2014, p. 012031. IOP Publishing
11. Ramu, N., Muralidharan, R., Meera, K., Jeong, Y.H.: Tailoring the magnetic and magnetoelectric properties of rare earth orthoferrites for room temperature applications. RSC Adv. **6**(76), 72295–72299 (2016)
12. Gildo-Ortiz, L., Reyes-Gómez, J., Flores-Álvarez, J.M., Guillén-Bonilla, H., Olvera, M.d.l.L., Betancourtt, V.M.R., Verde-Gómez, Y., Guillén-Cervantes, A., Santoyo-Salazar, J.: Synthesis, characterization and sensitivity tests of perovskite-type $LaFeO_3$ nanoparticles in CO and propane atmospheres. Ceram. Int. **42**(16), 18821–18827 (2016)
13. Bamzai, K.K., Bhat, M.: Electrical and magnetic properties of some rare earth orthoferrites ($RFeO_3$ where R= Y, Ho, Er) systems. Integr. Ferroelectr. **158**(1), 108–122 (2014)
14. Gaikwad, V.M., Sheikh, J.R., Acharya, S.A.: Investigation of photocatalytic and dielectric behavior of $LaFeO_3$ nanoparticles prepared by microwave-assisted sol-gel combustion route. J. Sol-Gel Sci. Technol. **76**(1), 27–35 (2015)
15. Ye, J.L., Wang, C.C., Ni, W., Sun, X.H.: Dielectric properties of $ErFeO_3$ ceramics over a broad temperature range. J. Alloys Compd. **617**, 850–854 (2014)
16. Deng, G., Guo, P., Ren, W., Cao, S., Maynard-Casely, H.E., Avdeev, M., McIntyre, G.J.: The magnetic structures and transitions of a potential multiferroic orthoferrite $ErFeO_3$. J. Appl. Phys. **117**(16), 164105 (2015). https://doi.org/10.1063/1.4919367
17. Hessien, M.M., Mersal, G.A.M., Mohsen, Q., Alosaimi, D.: Structural, magnetic and sensing properties of lanthanum ferrite via facile sol gel oxalate precursor route. J. Mater. Sci. Mater. Electron. **28**(5), 4170–4178 (2017)
18. Shen, H., Cheng, Z., Hong, F., Xu, J., Yuan, S., Cao, S., Wang, X.: Magnetic field induced discontinuous spin reorientation in $ErFeO_3$ single crystal. Appl. Phys. Lett. **103**(19), 192404 (2013)
19. Velhal, N.B., Patil, N.D., Shelke, A.R., Deshpande, N.G., Puri, V.R.: Structural, dielectric and magnetic properties of nickel substituted cobalt ferrite nanoparticles: effect of nickel concentration. AIP Adv. **5**(9), 097166 (2015)
20. Cao, S., Sinha, K., Zhang, X., Zhang, X., Wang, X., Yin, Y., Wang, J., Keavney, D.J., Paudel, T.R., Liu, Y.: Electronic structure and direct observation of ferrimagnetism in multiferroic hexagonal $YbFeO_3$. Phys. Rev. B. **95**(22), 224428 (2017)
21. Fawzi, A.S., Sheikh, A.D., Mathe, V.L.: Structural, dielectric properties and AC conductivity of $Ni_{(1-x)}Zn_xFe_2O_4$ spinel ferrites. J. Alloys Compd. **502**(1), 231–237 (2010)
22. Prathap, S., Madhuri, W.: Multiferroic properties of microwave sintered $PbFe_{12-x}O_{19-\delta}$. J. Magn. Magn. Mater. **430**, 114–122 (2017)